

Nanoparticulate origin of intrinsic residual stress in thin films

G. Guisbiers, O. Van Overschelde, M. Wautelet *

Physics of Condensed Matter, University of Mons-Hainaut, Avenue Maistriau 23, B-7000 Mons, Belgium

Received 6 October 2006; received in revised form 2 February 2007; accepted 4 February 2007

Available online 21 March 2007

Abstract

The formation of grains in thin films generates intrinsic residual stress. In this work, we present a model of intrinsic residual stress calculation based on the size-dependent phase transitions of the nanograins. Evaporated thin films are produced by condensation from the vapor on the substrate. It is assumed that the starting nanograins grow from the liquid phase. It is well established that the melting temperature of nanoparticles is a function of their size. By assuming that the intrinsic stress originates from the volume change of the nanograins, and taking into account relaxation processes, the generated intrinsic residual stress in the films is evaluated. The results of the model are compared quantitatively with experimental data obtained from Ta, Mo, Pd and Al films deposited on Si. This model also gives a theoretical interpretation of Thornton and Hoffman's modelling of the stress-temperature diagram of thin films.

© 2007 Acta Materialia Inc. Published by Elsevier Ltd. All rights reserved.

Keywords: Nanostructure; Grain size; Grain morphology; Residual stresses; Phase transformation

1. Introduction

When thin films are deposited on a substrate, residual stresses generally appear. Such stresses can lead to various effects: curvature of the system, detachment of films and modification of the performance of devices made with such systems, e.g. microelectronic or microelectromechanical systems. The study of residual stress therefore appears to be of tremendous importance [1]. Although the importance of stress is recognized, the fundamental mechanisms are far from being fully understood.

In the literature, three kinds of residual stress can be distinguished: intrinsic, thermal and external stress [1]. Intrinsic stresses are generated during the deposition process of thin films on their substrate. Thermal stress is caused by the difference between the thermal expansion coefficients of the substrate and the film material, and occurs especially during the cooling phase. External residual stresses are due to, for instance, oxidation and incorporation of impurities.

The origin of intrinsic stress is not yet fully understood [1]. In 1976, Hoffman [2] proposed estimating the intrinsic residual stress by assuming that the isolated grains pull together and form grain boundaries. Grains of radius R are assumed to be separated by a distance, δ , of the order of one interatomic distance. Hoffman then deduced that the intrinsic residual stress is given by $\sigma_{\text{intrinsic}} = (E_f/1 - \nu_f)(\delta/2R)$. This model is based on the existence of the parameter δ , which is difficult to calculate from first principles.

In 1999, Nix and Clemens [3] studied Hoffman's coalescence mechanism in thermodynamic terms. They obtained a relation for the maximum value of the stress: $\sigma_{\text{intrinsic_max}} = [(E_f/1 - \nu_f)(2\gamma_{SV} - \gamma_{GB})/R]^{1/2}$. In this equation, γ_{SV} and γ_{GB} are the surface tension of the isolated grains per unit area and the surface tension of the grain boundary per unit area, respectively. The main physical difficulty with this model is the determination of the parameter γ_{GB} .

Abermann and Koch obtained experimental data on residual stresses in thin metallic films [4–7]. They showed that thermal residual stress was negligible compared to intrinsic residual stress. According to Hoffman and

* Corresponding author.

E-mail address: Michel.Wautelet@umh.ac.be (M. Wautelet).

Thornton [2,8], the intrinsic residual stress component is highly temperature dependent and generally tensile [9,10]. The aim of the present work is to propose a model that can estimate intrinsic stress without using external adjustable parameters. It is based on the size dependence of the melting temperature of nanoparticles, which are assumed to be present at the early stage of film deposition on a substrate. The mechanisms of deposition and the origin of residual stresses are discussed in Section 2. The theoretical results are compared with previous experimental results in Section 3. Sections 4 and 5 deal with discussions and conclusions, respectively.

2. Model of thin film deposition

Let us consider the cases of thermal or electron-beam evaporated thin films on a substrate. At the start of deposition, atoms arrive on the substrate, where they are first adsorbed. Then the atoms move rapidly around on the surface and agglomerate to form nanosized grains. It is known that the melting temperature of nanoparticles, T_m , is lower than that of bulk material, $T_{m,\infty}$ [11–17]. Therefore, let us assume that the grains first grow in the liquid state [18,19]. When the grains grow above a critical size, they reach their solidification temperature. After a short period of induction ($t \approx 10^{-9}$ s) [20], they suddenly solidify. During solidification, the latent heat of melting is released and the grain remains liquid for some time. It is assumed here that the transient temperature reaches the melting temperature of the grain at the solidification size. The solid grain then rapidly cools down. This phase transition induces a volume change due to thermal contraction. This is the origin of the intrinsic residual stress [1,21–23]. Some relaxation takes place, giving rise to the observed intrinsic stress. Let us now develop these points.

2.1. Size-dependent melting temperature

Nanometer-sized particles are characterized by the fact that the ratio of the number of surface atoms to volume atoms is not small. It is then obvious that the effects of the surface on the cohesive properties of the particle cannot be neglected. This is seen in various situations, such as the well-known size-dependent melting point depression [11–17]. For inorganic materials, it is known that the spherical grain melting temperature, T_m , decreases linearly with R^{-1} , where R is the radius of the grain [11,12,16]:

$$\frac{T_m}{T_{m,\infty}} = 1 + \frac{3(\gamma_l - \gamma_s)}{R\Delta H_{m,\infty}} \quad (1)$$

where $T_{m,\infty}$ is the bulk melting point, $\Delta H_{m,\infty}$ the fusion enthalpy, and γ_l and γ_s are the surface tensions of the liquid and solid phases, respectively.

When the particle is not spherical (e.g. droplets or polyhedra on a surface), the melting point depression might be smaller or larger than for a spherical particle, depending on its shape [11,12,16]. In a previous work [16], it has been

demonstrated that, depending on the material deposited, some solid shapes are preferred. For instance, Ta, Mo and Pd adopt a spherical shape on Si, while Al grows as parallelepiped columns.

For a truncated tetrahedron on a substrate, the melting temperature is given by [16]:

$$\frac{T_m}{T_{m,\infty}} = 1 - \left[\frac{\frac{E_{\text{stress}}}{\pi R^2(1-\cos\theta_1)^2(2+\cos\theta_1)} + \frac{3\sqrt{3}a^2}{4\pi R^2(1-\cos\theta_1)^2(2+\cos\theta_1)} \gamma_s}{+ \frac{\sqrt{3}a^2}{4\pi R^2(1-\cos\theta_1)^2(2+\cos\theta_1)} \gamma_{s\beta} - \frac{(1+\cos\theta_1)}{(1-\cos\theta_1)(2+\cos\theta_1)} \gamma_\beta - \gamma_l} \right] \frac{3}{R\Delta H_{m,\infty}} \quad (2)$$

For a parallelepiped shape on a substrate, the melting temperature is given by [16]:

$$\frac{T_m}{T_{m,\infty}} = 1 - \left[\frac{\frac{E_{\text{stress}}}{\pi R^2(1-\cos\theta_1)^2(2+\cos\theta_1)} + \frac{2ah+bh+ab}{\pi R^2(1-\cos\theta_1)^2(2+\cos\theta_1)} \gamma_s}{+ \frac{ab}{\pi R^2(1-\cos\theta_1)^2(2+\cos\theta_1)} \gamma_{s\beta} - \frac{(1+\cos\theta_1)}{(1-\cos\theta_1)(2+\cos\theta_1)} \gamma_\beta - \gamma_l} \right] \frac{3}{R\Delta H_{m,\infty}} \quad (3)$$

It is worth noting that, due to thermodynamic arguments, Eqs. (1)–(3) are valid when $R > 2-3$ nm [11,12,16]. The melting temperatures of nanograins of various elements are given in Table 1.

2.2. Intrinsic residual stress

As mentioned above, during the deposition process, the nanosized grains are assumed to be initially in the liquid state [18,19]. When they grow, they attain a critical size, R_c , which is reached when the deposition temperature is equal to the melting temperature. Solidification does not take place immediately. It is well established that there is an induction period before the appearance of phase transitions [17,20,24]. During this period, the grain grows, and hence its melting temperature increases. Therefore, solidification takes place for $R \geq R_c$. When the phase transformation takes place, the latent heat of solidification is released into the system. This heat release takes place over a very short time, hence it is reasonable to assume that this leads to the heating of the grain up to the melting temperature at R . The intrinsic stress would then be due to the quenching of the solidified grain from the melting temperature to the substrate temperature. Assuming that the solid film adheres to the substrate and that it is in a biaxial stress state, the relation between strain and stress is given by [23]:

$$\sigma_0 = \frac{E_f}{1 - \nu_f} \Delta \varepsilon \quad (4)$$

In this equation, E_f and ν_f are respectively the Young's modulus and the Poisson's ratio of the deposited material. In the present work, it is assumed that the strain is due to the size-dependent liquid–solid phase transition, via the following equation [23]:

$$\Delta \varepsilon = \alpha_f (T_m - T_{\text{substrat}}) \quad (5)$$

Table 1

Melting temperature of the nanograin, relaxation time, initial intrinsic residual stress and final intrinsic residual stress

Material (radius)	T_m (K)	t (s)	σ_0 (MPa)	σ (MPa)
<i>Spherical shape</i>				
Ag (2 nm)	654	7.35×10^{-14}	893	176
Ag (5 nm)	1002	4.79×10^{-14}	1757	609
Ag (10 nm)	1119	4.30×10^{-14}	2045	792
Au (2 nm)	726	6.62×10^{-14}	824	316
Au (5 nm)	1093	4.40×10^{-14}	1523	805
Au (10 nm)	1215	3.95×10^{-14}	1755	990
Cr (2 nm)	1361	3.53×10^{-14}	1392	237
Cr (5 nm)	1853	2.59×10^{-14}	2032	554
Cr (10 nm)	2016	2.38×10^{-14}	2245	680
Co (2 nm)	667	7.21×10^{-14}	1497	70
Co (5 nm)	1327	3.62×10^{-14}	4146	890
Co (10 nm)	1548	3.10×10^{-14}	5028	1344
Cu (2 nm)	805	5.97×10^{-14}	1638	169
Cu (5 nm)	1137	4.23×10^{-14}	2699	540
Cu (10 nm)	1247	3.85×10^{-14}	3053	704
Fe (2 nm)	698	6.88×10^{-14}	1480	107
Fe (5 nm)	1366	3.52×10^{-14}	3921	1025
Fe (10 nm)	1588	3.02×10^{-14}	4735	1493
Hf (2 nm)	1486	3.23×10^{-14}	1368	570
Hf (5 nm)	2098	2.29×10^{-14}	2070	1113
Hf (10 nm)	2302	2.09×10^{-14}	2304	1308
Ir (2 nm)	2063	2.33×10^{-14}	8588	1483
Ir (5 nm)	2457	1.96×10^{-14}	10,497	2402
Ir (10 nm)	2588	1.86×10^{-14}	11,134	2745
Mn (2 nm)	907	5.30×10^{-14}	3641	52
Mn (5 nm)	1274	3.77×10^{-14}	5819	284
Mn (10 nm)	1397	3.44×10^{-14}	6545	417
Mo (2 nm)	2127	2.26×10^{-14}	4692	992
Mo (5 nm)	2586	1.86×10^{-14}	5868	1635
Mo (10 nm)	2740	1.75×10^{-14}	6260	1874
Ni (2 nm)	1053	4.56×10^{-14}	3224	433
Ni (5 nm)	1458	3.29×10^{-14}	4941	1160
Ni (10 nm)	1593	3.02×10^{-14}	5513	1463
Nb (2 nm)	1713	2.80×10^{-14}	1749	888
Nb (5 nm)	2335	2.06×10^{-14}	2514	1529
Nb (10 nm)	2543	1.89×10^{-14}	2770	1754
Os (2 nm)	2619	1.84×10^{-14}	10,573	2452
Os (5 nm)	3031	1.59×10^{-14}	12,448	3522
Os (10 nm)	3169	1.52×10^{-14}	13,073	3907
Pd (2 nm)	1058	4.54×10^{-14}	1699	457
Pd (5 nm)	1520	3.16×10^{-14}	2726	1092
Pd (10 nm)	1674	2.87×10^{-14}	3068	1337
Pt (2 nm)	1266	3.80×10^{-14}	2440	938
Pt (5 nm)	1731	2.78×10^{-14}	3607	1793
Pt (10 nm)	1886	2.55×10^{-14}	3996	2104
Re (2 nm)	2158	2.23×10^{-14}	8689	1739
Re (5 nm)	2938	1.64×10^{-14}	12,322	3781
Re (10 nm)	3198	1.50×10^{-14}	13,534	4571
Rh (2 nm)	1494	3.22×10^{-14}	5237	445
Rh (5 nm)	1940	2.48×10^{-14}	7181	1076
Rh (10 nm)	2088	2.30×10^{-14}	7829	1343
Ru (2 nm)	1938	2.48×10^{-14}	8623	1093

Table 1 (continued)

Ru (5 nm)	2340	2.05×10^{-14}	10,730	1938
Ru (10 nm)	2473	1.94×10^{-14}	11,430	2265
Sc (2 nm)	725	6.62×10^{-14}	451	22
Sc (5 nm)		3.49×10^{-14}	11,34	233
Sc (10 nm)	1596	3.01×10^{-14}	1361	348
Ta (2 nm)	2007	2.39×10^{-14}	3240	1529
Ta (5 nm)	2777	1.73×10^{-14}	4694	2728
Ta (10 nm)	3033	1.58×10^{-14}	5179	3151
Ti (2 nm)	1077	4.46×10^{-14}	1027	229
Ti (5 nm)	1595	3.01×10^{-14}	1706	620
Ti (10 nm)	1768	2.72×10^{-14}	1933	775
W (2 nm)	2523	1.90×10^{-14}	5433	1503
W (5 nm)	3225	1.49×10^{-14}	7143	2614
W (10 nm)	3459	1.39×10^{-14}	7713	3021
V (2 nm)	1332	3.61×10^{-14}	1711	460
V (5 nm)	1843	2.61×10^{-14}	2552	987
V (10 nm)	2013	2.39×10^{-14}	2832	1187
Zr (2 nm)	1114	4.31×10^{-14}	512	226
Zr (5 nm)	1722	2.79×10^{-14}	892	525
Zr (10 nm)	1925	2.50×10^{-14}	1018	634
<i>Parallelepiped shape</i>				
Al (2 nm)	621	7.73×10^{-14}	804	16
Al (5 nm)	808	5.94×10^{-14}	1262	61
Al (10 nm)	871	5.52×10^{-14}	1415	85
Y (2 nm)	975	4.93×10^{-14}	657	163
Y (5 nm)	1467	3.28×10^{-14}	1130	448
Y (10 nm)	1631	2.95×10^{-14}	1288	560
Zn (2 nm)	654	7.34×10^{-14}	1179	117
Zn (5 nm)	677	7.09×10^{-14}	1254	135
Zn (10 nm)	685	7.01×10^{-14}	1279	141

where α_f is the thermal expansion coefficient of the deposited material and σ_0 is the initial stress. Some stress-relaxation takes place; for metallic coatings, yielding is one of the major stress-relaxation mechanisms [25]. During the liquid–solid phase transition, let us assume the grain behaves viscoelastically. The stress-relaxation equation is then given by [10,26]:

$$\sigma_{\text{intrinsic}}(t) = \sigma_0 \exp\left(\frac{-E_f t}{\eta_f}\right) \quad (6)$$

It is worth noting that the viscosity concept remains valid at the nanometer scale [27]. Assuming that the whole thermal energy of the nanograin is relaxed by vibrations of the atoms constituting the nanograin when it solidifies on the substrate, the vibration frequency of the atoms is evaluated by Eq. (7) via the nanograin melting temperature:

$$k_b T_m = h_p \nu \quad (7)$$

Inverting the vibration frequency of the atoms, the relaxation time t can be deduced by [28]:

$$t = 1/\nu \quad (8)$$

Knowing the melting temperature of the nanograin from Eqs. (1)–(3), Eqs. (4)–(8) allows the intrinsic stress to be calculated.

2.3. Total residual stress

The total residual stress is the sum of the intrinsic, thermal and external stresses. Let us assume that the external stress is negligible. The thermal stress results from the lattice constant modifications when cooling from the deposition temperature to the ambient temperature. This stress is given by [1]:

$$\sigma_{\text{thermic}} = (E_f/1 - \nu_f)\Delta\alpha\Delta T \quad (9)$$

where ΔT is the difference between the deposition temperature and the ambient temperature and $\Delta\alpha$ is the difference between the thermal expansion coefficients of the substrate and the thin film. The experimental evaluation of this term requires knowing the exact deposition temperature.

2.4. Theoretical results

The model allows the intrinsic residual stress inside the nanograin before the coalescence of the thin film to be calculated. The residual stress is maximum at the coalescence stage [9]. Then the stress relaxes due to coalescence caused by atomic diffusion, dislocations and fractures. Table 1 gives the values of the intrinsic residual stress of various elements for different grain sizes. It turns out that this stress increases with increasing radius, in accordance with other work [29].

3. Comparison with experimental data

In order to evaluate the validity of the present theoretical model, the results were compared with previous experimental work on Ta, Mo, Pd and Al films deposited by electron-beam evaporation on Si substrates [30,31]. The

curvature of the samples was measured by laser deflection. The total residual stress was deduced by means of Stoney's equation. Let us recall that one needs to know the deposition temperature in order to compare the experimental and theoretical data. Since we deal with the situation at the start of the deposition process, experimental data obtained at low film thickness (100 nm) are given. As mentioned above, the present theoretical model is valid prior to coalescence, i.e. gives an upper limit for the measured stress.

In a first step, the thermal residual stress is calculated via Eq. (9). This is then deducted from the total residual stress in order to obtain the intrinsic residual stress. The results are given in Table 2. It turns out that our model fits the experimental data, for $R \approx 1.5$ nm, in the case of Ta, Mo and Pd.

In the case of Al, given the uncertainty in the experimental data and the fact that the residual stress is low, we can conclude only that the correct order of magnitude is obtained.

It is also worth noting that the present model accounts for the differences between Al and Ta, Mo and Pd.

4. Discussion

In Fig. 1a, the variation of $\sigma_{\text{intrinsic}}$ with the melting temperature of the elements (given in Table 1) is plotted. It turns out that $\sigma_{\text{intrinsic}}$ increases with increasing T_m . These variations fit very well with the following relations:

$$\sigma_{\text{intrinsic}} = 0.96T_m - 651.05 \quad \text{when } R = 2 \text{ nm} \quad (10)$$

$$\sigma_{\text{intrinsic}} = 1.27T_m - 1037.57 \quad \text{when } R = 5 \text{ nm} \quad (11)$$

$$\sigma_{\text{intrinsic}} = 1.35T_m - 1142.27 \quad \text{when } R = 10 \text{ nm} \quad (12)$$

In Fig. 1b, $\sigma_{\text{intrinsic}}$ is plotted vs. the ratio $T_{\text{substrate}}/T_m$ where the temperature of the substrate $T_{\text{substrate}}$ is taken as 293.15 K [30,31]. This allows us to give a theoretical interpretation of the empirical criteria given by Thornton and Hoffman [8]. These authors divide the materials into

Table 2

Ratio between the substrate temperature and the melting temperature of the nanograins, the prediction of Thornton and Hoffman's criteria at the macroscale, and the intrinsic and thermal residual stress

Samples	$T_{\text{substrate}}/T_{m,\infty}$	$\sigma_{\text{domination}}$ according Thornton and Hoffman at the macroscale	$\sigma_{\text{intrinsic}}$ (MPa)	σ_{thermic} (MPa)
Ta 100 nm	0.11	Intrinsic	781 (97%)	22 (3%)
Ta 200 nm	0.12	Intrinsic	488 (92%)	45 (8%)
Ta 400 nm	0.11	Intrinsic	192 (85%)	34 (15%)
Ta 600 nm	0.13	Intrinsic	76 (55%)	62 (45%)
Mo 100 nm	0.12	Intrinsic	420 (99%)	6 (1%)
Mo 200 nm	0.12	Intrinsic	550 (99%)	6 (1%)
Mo 400 nm	0.12	Intrinsic	596 (99%)	8 (1%)
Mo 600 nm	0.12	Intrinsic	327 (98%)	7 (2%)
Pd 100 nm	0.17	Intrinsic	587 (94%)	37 (6%)
Pd 200 nm	0.17	Intrinsic	719 (93%)	51 (7%)
Pd 400 nm	0.17	Intrinsic	794 (93%)	60 (7%)
Pd 600 nm	0.18	Intrinsic	520 (77%)	152 (23%)
Al 100 nm	0.32	Thermal	68 (92%)	6 (8%)
Al 200 nm	0.32	Thermal	33 (80%)	8 (20%)
Al 400 nm	0.32	Thermal	8 (50%)	8 (50%)
Al 600 nm	0.32	Thermal	2 (13%)	13 (87%)

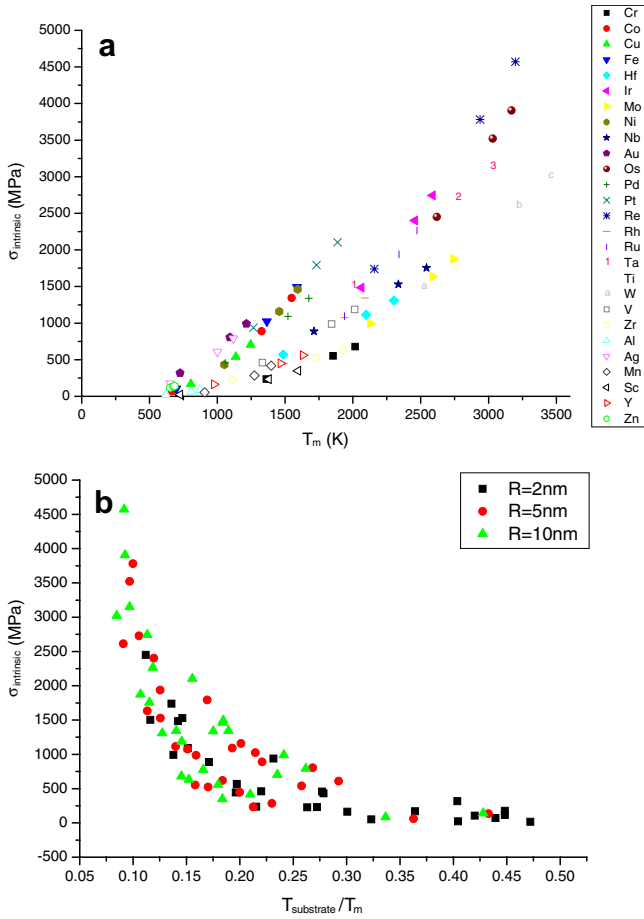


Fig. 1. (a) Intrinsic residual stress vs. the melting temperature of the nanograin. The colors differentiate the materials. (b) Intrinsic residual stress vs. the ratio between the substrate temperature and the melting temperature of the nanograin. The colors differentiate the size. (For interpretation of the references in color in this figure legend, the reader is referred to the web version of this article.)

two main classes [8]. When $T_{\text{substrate}}/T_{m,\infty} > 0.25$ (low melting point), the materials are characterized by a low intrinsic residual stress (as compared with the thermal stress). When $T_{\text{substrate}}/T_{m,\infty} < 0.25$ (high melting point), the materials are characterized by a high intrinsic residual stress.

Analysing Table 2, Thornton and Hoffman’s criteria predict a domination of thermal stress over intrinsic stress for the 100 and 200 nm Al samples (Fig. 2); however, this is not the case experimentally [30,31]. Therefore, Thornton and Hoffman’s criteria need to be adapted for the nanoscale such that the separation point is a function of R . To quantitatively separate the low and high intrinsic residual stress regimes, let us define that the separation between these two regimes occurs when ; with this definition it is certain that when separation occurs the thermal stress will dominate the intrinsic stress. So replacing $\sigma_{\text{intrinsic}}$ by 0 in Eqs. (10)–(12), we determine the ratio $T_{\text{substrate}}/T_m$ when the separation occurs for each size. When $R = 2, 5$ and 10 nm the separation is respectively deduced to take place at $T_{\text{substrate}}/T_m = 0.43, 0.36$ and 0.35 . Plotting these results

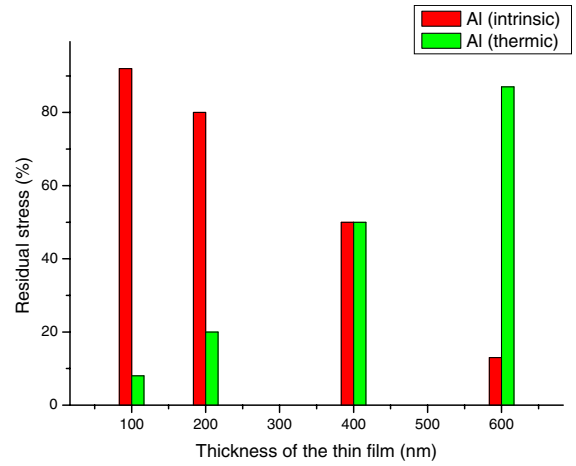


Fig. 2. Intrinsic and thermal residual stress (%) vs. the thickness of the Al thin film. The total residual stress corresponds to 100%.

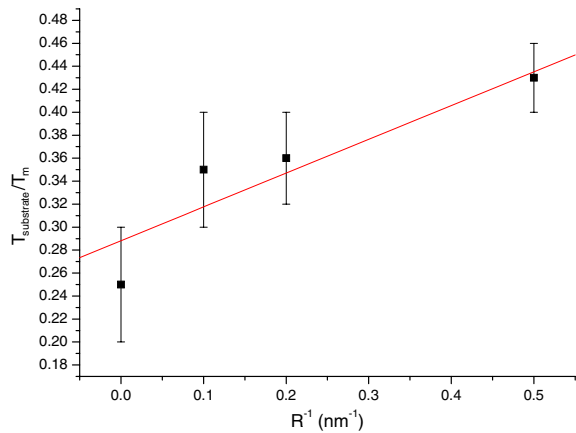


Fig. 3. Ratio of the substrate temperature to the melting temperature of the nanograin $T_{\text{substrate}}/T_m$ vs. R^{-1} .

in Fig. 3, it turns out that the separation point is given by the following equation:

$$T_{\text{substrate}}/T_m = 0.28 + 0.31R^{-1} \quad (13)$$

Thus Thornton and Hoffman’s criteria adapted for the nanoscale predict the domination of the intrinsic residual stress over the thermal stress for the 100 and 200 nm Al samples. They also predict the domination of the intrinsic stress over the thermal stress for all the Ta, Mo and Pd samples and the domination of the thermal stress over the intrinsic stress for the 400 and 600 nm Al samples, in accordance with the experimental data.

Eq. (13) describes the modification of Thornton and Hoffman’s criteria when the size of the nanograins reduces. This allows us to quantify Thornton and Hoffman’s criteria.

5. Conclusions

The present model permits quantitative evaluation of the intrinsic residual stress of a thin film during the first steps of deposition, before coalescence. It is based on the

variation of the melting temperature of nanograins with their size. Its main interest is that it needs no external parameter. Further work is obviously needed in order to verify the validity of the basic assumptions of our model, such as the fact that the nanograins first grow in the liquid state and that the critical radius is in the 1–2 nm range. The model also explains the origin of Thornton and Hoffman's criteria at the nanoscale.

Acknowledgement

This work is partially supported by Project MOMIOP (Walloon Region – Belgium).

Appendix

α_f	is the thermal expansion coefficient of the deposited material (K^{-1})
E_f	is the Young modulus of the deposited material (Pa), E_{stress} is the parameter taking into account the influence of the substrate (J)
$\Delta\varepsilon$	is the strain due to the phase transition (–)
γ_l and γ_s	are the surface tensions of the liquid and solid phases, respectively (J m^{-2})
$\Delta H_{m,\infty}$	is the fusion enthalpy (J m^{-3})
h_p	is the Planck's constant (J s)
k_b	is the Boltzmann's constant (J K^{-1})
η_f	is the viscosity of the deposited material (Pa s)
θ_l	is the contact angle of the liquid droplet on the substrate (°)
σ_0	is the initial stress due to the liquid–solid phase transition (Pa)
$T_{m,\infty}$	is the bulk melting temperature (K)
T_m	is the nanograin melting temperature (K)
$T_{\text{substrate}}$	is the substrate temperature (K)
t	is the relaxation time (s)
ν	is the vibration frequency of the atoms in the nanograin (Hz)
ν_f	is the Poisson's ratio of the deposited material (–)

References

- [1] Madou MJ. Fundamentals of microfabrication: the science of miniaturization. 2nd ed. Boca Raton, FL: CRC Press; 2002. p. 262.
- [2] Hoffman RW. Thin Solid Films 1976;34:185.
- [3] Nix WD, Clemens BM. J Mater Res 1999;14:3467.
- [4] Abermann R, Koch R. Thin Solid Films 1985;129:71.
- [5] Koch R, Abermann R. Thin Solid Films 1986;140:217.
- [6] Koch R, Abermann R. Thin Solid Films 1985;129:63.
- [7] Koch R. J Phys Condens Mat 1994;6:9519.
- [8] Thornton JA, Hoffman DW. Thin Solid Films 1989;171:5.
- [9] Doerner MF, Nix WD. CRC Crit Rev Sol State Mater Sci 1988;14:225.
- [10] Ohring M. Materials science of thin films, deposition and structure. 2nd ed. New York: Academic Press; 2002. p. 743.
- [11] Wautelet M. Phys Lett A 1998;246:341.
- [12] Wautelet M. Eur Phys J Appl Phys 2005;29:51.
- [13] Takagi M. J Phys Soc Jap 1986;55:3484.
- [14] Nanda KK, Sahu SN, Behera SN. Phys Rev A 2002;66:013208.
- [15] Zhao M, Zhou XH, Jiang Q. J Mater Res 2001;16:3304.
- [16] Guisbiers G, Wautelet M. Nanotechnology 2006;17:2008.
- [17] Sun CQ, Tay BK, Zeng XT, Li S, Chen TP, Zhou J, et al. J Phys: Condens Mat 2002;14:7781.
- [18] Storozhev VB. Surf Sci 1998;397:170.
- [19] Petrov I, Barna PB, Hultman L, Greene JE. J Vac Sci Technol 2003;A21:117.
- [20] Bäuerle D. Laser processing and chemistry. 3rd ed. Berlin: Springer-Verlag; 2000. p. 174.
- [21] Murbach HP, Wilman H. Proc Phys Soc 1953;66B:905.
- [22] Murbach HP, Wilman H. Vacuum 1954;4:109.
- [23] Guisbiers G, Monteverde F, Leclère Ph, Lazzaroni R, Van Overschelde O, Wautelet M. Mater. Sci. Eng. A [submitted for publication].
- [24] Somorjai GA, Delplancke MP. Chimie des surfaces et catalyse. Ediscience International; 1995. p. 316.
- [25] Tsui YC, Clyne TW. Thin Solid Films 1997;306:23.
- [26] Chen KS, Zhang X, Lin SY. Thin Solid Films 2003;434:190.
- [27] Bhushan B et al. Handbook of nanotechnology. Berlin: Springer-Verlag; 2004. p. 581.
- [28] Chopra KL. Thin film phenomena. New York: McGraw-Hill; 1969. p. 139.
- [29] Lee BJ, Lee CS, Lee JC. Acta Mater 2003;51:6233.
- [30] Guisbiers G, Strehle S, Wautelet M. Microelec Eng 2005;82:665.
- [31] Guisbiers G, Strehle S, Van Overschelde O, Wautelet M. In: AIP proceedings of 8th international workshop on stress induced phenomena in metallization, vol. 817. Dresden, Germany; 2005. p. 317.